



## Lateral constrained wrinkling of the film with partial contact

Mengxiong Liu <sup>a,b</sup>, Zhiming Xue <sup>c,d</sup>, Yafei Wang <sup>c,d</sup>, Xide Li <sup>a,b</sup>, Changguo Wang <sup>c,d,\*</sup>

<sup>a</sup> Department of Engineering Mechanics, Tsinghua University, Beijing 100084, China

<sup>b</sup> Center for Nano and Micro Mechanics, Tsinghua University, Beijing 100084, China

<sup>c</sup> Center for Composite Materials, Harbin Institute of Technology, Harbin, China, 150001

<sup>d</sup> National Key Laboratory of Science and Technology for National Defence on Advanced Composites in Special Environments, Harbin Institute of Technology, Harbin 150080, China



### ARTICLE INFO

#### Keywords:

Film wrinkling  
Partial contact and interface fracture  
Lateral constraints  
Geometrical and contact nonlinearities

### ABSTRACT

This paper establishes three analytical models, including the interface bonded type (B-type), interface sliding type (S-type) and the lateral constrained type (C-type), to reveal the effects of the partial contact and lateral constraints on the film wrinkling behaviors. Due to the geometrical and contact nonlinearities, a numerical method is applied to solving the displacement and stress fields, and the shear-lag effect caused by contact is included. The deformation of the film can be characterized by 5 processes, firstly compressing (I), secondly wrinkling (II), then the growing of wrinkled part giving rise to point contact (III), line contact (IV), and finally mode transition(V), which are verified by a demonstrative experiment. Moreover, effects of the contact parameters, including the interfacial strength, interfacial stiffness and the initial contact region length, on the deformation of the film are analyzed. Finally, the established models are applied to characterize the wrinkling behaviors of a graphene contacting to the polyethylene terephthalate (PET). The minimum pre-existing defect size for graphene wrinkling is 7 nm, less than which the interface failure precedes the film wrinkling. The critical wrinkling strain shows significant size effect when the graphene length is less than 13 μm, where all the interfaces participate the load transfer. The obtained results are consistent with the experimental and the numerical data given in the references, where the differences are also discussed detailly.

### 1. Introduction

When subjected to the uniform compression, a film bonded on the substrate can be wrinkled and present different instability morphologies [2,3,15,19,20,33,42,43,47]. Such a film/substrate system has been extensively studied due to its potential application in many interesting fields, including the stretchable electronics [26], the micro/nano-fabrications [38] and the mechanical properties measurements of films [36]. However, the assumption of the continuous bonding between the film and the substrate is not always suitable for most of the film/substrate system. Especially, in the practical applications, the interface defects [41], the local delamination [17] and the partially discrete bonding [9] are more common. Taking the stretchable electronics for example, the Si/Ferroelectric nanoribbons are integrated on the discontinuous elastomeric substrates, where the discrete interface bonding results in the “wavy” configurations of the soft supports to achieve reversible, linear elastic responses to large strain deformations [12,21]. Because the interface of the film and the substrate with

discontinuous bonding is similar to the partial contact usually meaning that two objects are not in full contact in the references [25,31,40], the film partially making contact with the substrate is called as the partial contact condition. How to evaluate the effect of the partial contact on the film wrinkling is important.

For the film with the partial contact interface, one of the very common phenomena is the interfacial sliding [7,14,24]. It is always considered as the disastrous consequences for the film/substrate system because the structures will automatically fail once the interfacial sliding appears [10,11,34]. For the stretchable and flexible electronics formed by the inorganic films and the plastic substrate, interfacial slippage is very dangerous because it often occurs before material rupture when subjected to repeated bending or stretching in application [11]. On the other hand, the interfacial sliding can be fully utilized by characterizing the wrinkles formed by the film [39,23]. For example, in the silicone rubber/cell system, the traction force between cells and the silicone film can be visualized by film wrinkling when tissue cells move forward and the intrinsic properties of such film can also be estimated by cells’

\* Corresponding author.

E-mail address: [wangcg@hit.edu.cn](mailto:wangcg@hit.edu.cn) (C. Wang).

locomotion [1,32]. However, due to the introduction of the interfacial sliding, variety of problems are involved, including the predictions of the critical wrinkling stress/strain, the stress/strain transfer mechanism at the interface, and the evolution of the sliding and wrinkling [6,44,46]. Thus, it is crucial to comprehensively evaluate the effect of the interfacial sliding on the film wrinkling when contacting with the substrate.

Mostly, the surrounding of the film is not a free space but a constrained one in practical application (Zhang et al., 2018; [4,13]). Thus, the lateral constraints for the film deformation in most cases are very common and the wrinkle formed by the film can make contact with the surrounding environment or the substrate. For the Si nanoribbons/micro-patterned substrate system used as the stretchable electronic, the downward buckles will appear by tuning the micro-patterns and then make contact with the substrate (Zhang et al., 2018). Moreover, the lateral constrained film wrinkling is an important issue in the application of the Lithium-ion batteries (LIBs). After encapsulation, wrinkles formed by the solid-electrolyte interphase (SEI) layer will be constrained by the surrounding environment [29,30]. Thus, when the lateral constrained space is introduced, some new question may arise. For example, what will happen to the configuration of wrinkles and what will happen to the mechanism of interface load transfer? Therefore, it is essential to include the effect of the lateral constraints in the film wrinkling.

Although the critical wrinkling strain of the film/substrate system is predicted in Hutchinson and Suo's work [22], the film is perfectly bonded to substrate there and the interfacial sliding is not considered. The interfacial sliding is often considered in some practical cases [7,11, 14,24,39,23], where the continuous interface bonding is always assumed. In addition, the effects of the lateral constraints are generally discussed for the column, plates, beams and balloon (Zhang et al., 2018; [5,29]), very little research has focused on the film wrinkling, especially when the partial contact is involved. However, in practical applications, the film wrinkling, the partial contact, the interfacial sliding and the lateral constraint always exist simultaneously ([1,5,23]; Zhang et al., 2018). They interact on each other, making the problem so complicated. More importantly, two nonlinear behaviors of the structural mechanics are involved in this problem, including the geometry and the contact nonlinearities. When wrinkles appear, the geometry nonlinearity should be considered to describe the large deformation behavior of the film [18, 22]. After the interfacial sliding is introduced, boundaries of the contact region will change and then the contact nonlinearity is included [11,23, 39]. Moreover, due to the lateral constrained space, wrinkles will make contact with the surrounding environment or the substrate and the configuration of wrinkles will change greatly with the increase of the contact region, where the contact nonlinearity is also included [4].

Based on investigations of the existing literature and the considerations mentioned above, assumptions of the typical film/substrate system need to be further released in the practical application, including the continuously desired bonding, the perfect bonding interface and the free space in surroundings. In this paper, the partial contact interface, the interfacial sliding and the lateral constraint are all involved to study the wrinkling behaviors of the film. This paper is organized as follows. In Section 2, three analytical models, including the B-type, S-type and C-type ones, are established, where the assumptions of the continuously desired bonding, the perfect bonding interface and the free space in surroundings are released one by one. Deformations of the film and the change of the interface are then characterized analytically by a set of governing equations. In Section 3, due to the double nonlinearity, the solving ideas are designed and the numerical solutions are performed. Section 4 is devoted to illustrate the effect of the interfacial strength, the interfacial stiffness and the initial contact region length on the wrinkling of the film. Then, wrinkling behaviors of the graphene contacting with the polyethylene terephthalate (PET) are characterized using our analytical models and compare with the results in the references. Finally, the paper ends up with some remarkable conclusions.

## 2. Model formulation

### 2.1. Description of the model

In the current work, we investigate the wrinkling behaviors of an isotropic film in contact with an elastic substrate, where the partial contact and the lateral constraint are considered. This work, as shown in Fig. 1(a), starts with the bonded interface called as the B-type, where the imperfection is introduced in the middle.

By replacing the perfect bonding at the interface with interfacial sliding, as shown in Fig. 1(b), the shear-lag effect is analyzed. And considering that the interfacial interactions may be the ligand-receptor bonds for silicone rubber/cell system [16,35] or the van der Waals interactions for graphene/substrate [8,9] and Cu/X ( $X = W$ , Nb or Zr) [37], the local springs are introduced to simplify the friction and adhesion interactions between film and substrate. For simplicity, this case is named as the S-type. Further, as shown in Fig. 1(c), the assumption of the free lateral space is released and the rigid plates are set as the constraints, which is called the C-type. The geometric and elastic parameters of the film and the elastic substrate are  $l_f \times b_f \times h_f E_f \nu_f$  and  $l_s \times b_s \times h_s E_s \nu_s$ , respectively. The distance between the film and the rigid plates in Fig. 1(c) is  $h$  and the length of the imperfection is  $b$ . Moreover, the local springs are assumed as the shear springs here because the shear direction is more prone to failure when the film contacts to the substrate [8,9,16,35,37]. The elastic constant of the spring is  $k$  and the area number density is  $\rho$ .

To understand the interfacial stress transfer, the classical shear-lag analysis is introduced to perform the studies on the simplified 2D unit cell shown in Fig. 2(a). As shown in this figure,  $x_A, x_B$  and  $x_C, x_D$  are the boundary coordinates of the film and the elastic substrate in the contact region, respectively. Here, the contact region means the region that the film makes contact with the elastic substrate. This model is based on the differential formulation in mechanics and the stress state of an infinitesimal element is shown in Fig. 2(b). Here, although the axial stress of the substrate is not evenly distributed across its thickness, it is considered as a constant in the elastic substrate surface. Based on the stress state shown in Fig. 2(b), the equilibrium equations of the film and the elastic substrate surface can be established in the contact region and non-contact region, respectively.

The elastic substrate surface:

$$\begin{cases} \text{contactregion : } h_s \frac{d\sigma_s}{dx} = \tau x_C \leq x \leq x_D \\ \text{non - contactregion : } \sigma_s = C_1 0 \leq x < x_C \end{cases}, \quad (1)$$

The film:

$$\begin{cases} \text{contactregion : } h_f \frac{d\sigma_f}{dx} + \tau = 0 x_A \leq x \leq x_B \\ \text{non - contactregion : } \sigma_f = C_2 0 \leq x < x_A \end{cases}, \quad (2)$$

where  $\tau = \rho k(u_s - u_f)$  and the subscripts f and s represent the film and the surface of the elastic substrate, respectively.  $u_f$  and  $u_s$  are the displacements of the film and the substrate surface in the contact area. According to the assumptions that the ligand-receptor bonds for silicone rubber/cell system [35] or the van der Waals interactions for graphene/substrate [8] will fail when the displacement differences of the cell and rubber or the graphene and substrate are greater than the critical values, the local springs in our models will break when the displacement differences ( $u_s - u_f$ ) of the film and the elastic substrate in the contact region are greater than the critical failure displacement ( $\delta_c$ ).

### 2.2. Description of the B-type model

For the bonded interface with prefabricated imperfections, as shown in Fig. 1(a), the analytic solution can be obtained when treating the film as a free-standing sheet with clamped edges [22,41,45]. With the

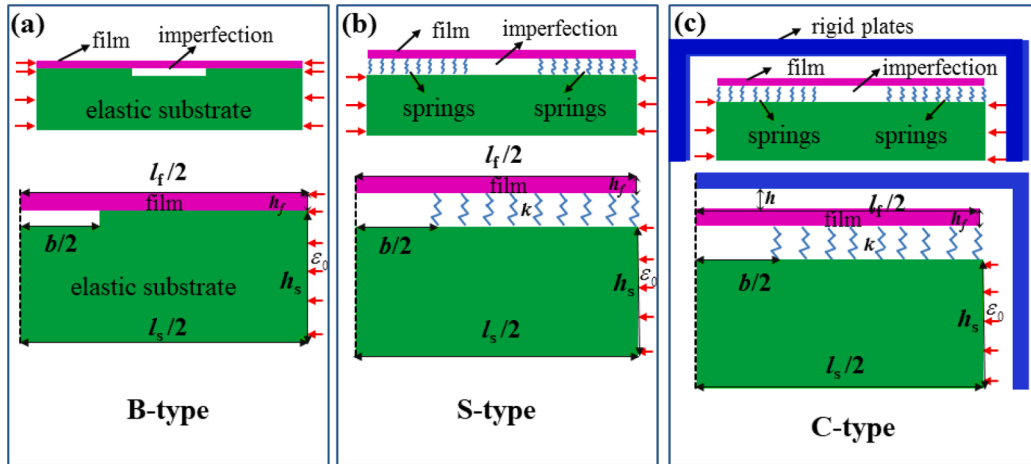


**Fig. 1.** (a) illustrates the bonded interface with pre-existing imperfection called as B-type. (b) shows the sliding interface named as S-type. (c) indicates the constrained lateral space called as C-type.

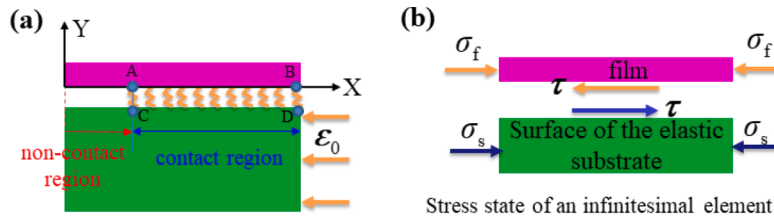


**Fig. 2.** Schematic of the 2D unit cell considering interfacial sliding. (a) shows the coordinates of the characteristic points. (b) is the stress state of an infinitesimal element.

increase of the compressive strain  $\varepsilon_0$ , the film will bifurcate from original flat state to the wrinkling one. Then, the amplitude of the wrinkles increases with further compressive strain. Here, the load is applied to both the film and the substrate. Thus, the stress at the film boundary (point B in Fig. 2(a)) equals to the applied load and the analytical solution of the film deformation can be obtained [22,41]. The critical wrinkling strain  $\varepsilon_c$  and the configuration of the wrinkle  $w$  can be expressed by Eq. (3) and Eq. (4).

$$\varepsilon_c = \frac{\pi^2}{12} \left( \frac{h_f}{x_A} \right)^2, \quad (3)$$

$$w = \frac{h_f}{\sqrt{3}} \left( 1 + \cos \left( \frac{x}{x_A} \right) \right) \sqrt{\frac{\varepsilon_0}{\varepsilon_c} - 1}, \quad (4)$$

### 2.3. Description of the S-type model

The shear-lag model is adopted here to study the effect of interfacial sliding on the deformation of the system. Increasing the compressive strain, as shown in Fig. 3, the film deformation will proceed through two phases: first flat compressing (Fig. 3(b)) and then wrinkling one (Fig. 3(c)).

Firstly, as shown in Fig. 3(b), the compressed process is analyzed. When the compressive strain  $\varepsilon_0$  is applied to the substrate, the film will

be compressed due to the stretched springs. In this process, the Cauchy strain ( $\varepsilon_s = \frac{du_s}{dx}, \varepsilon_f = \frac{du_f}{dx}$ ) is introduced to describe the deformation of the substrate surface and the film since only the in-plane deformation is considered here. Based on the small deformation assumption and the linear-elastic constitutive relation ( $\sigma_s = E_s \varepsilon_s, \sigma_f = E_f \varepsilon_f$ ), the equilibrium equations of the elastic substrate surface (Eq. (1)) and the film (Eq. (2)) in the contact region can be rewritten as:

$$\text{substratesurface : } h_s E_s \frac{d^2 u_s}{dx^2} = \rho k (u_s - u_f) x_C \leq x \leq x_D. \quad (5a)$$

$$\text{film : } h_f E_f \frac{d^2 u_f}{dx^2} + \rho k (u_s - u_f) = 0 x_A \leq x < x_B. \quad (5b)$$

Eq. (5) can be simplified as a four-order ordinary differential equation by replacing  $u_f$  with  $u_s$ .

$$\frac{d^4 u_s}{dx^4} - \frac{\rho k}{h_s E_s} \left( 1 + \frac{h_s E_s}{h_f E_f} \right) \frac{d^2 u_s}{dx^2} = 0 x_C \leq x \leq x_D. \quad (6)$$

By substituting  $\beta$  for  $\frac{\rho k}{h_s E_s} \left( 1 + \frac{h_s E_s}{h_f E_f} \right)$ , the general solution of this homogeneous ordinary differential equation can be obtained as.

$$u_s = a_c + b_c x + c_c e^{\sqrt{\beta} x} + d_c e^{-\sqrt{\beta} x} x_C \leq x \leq x_D. \quad (7a)$$

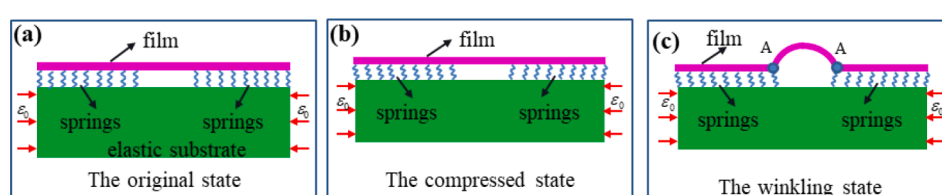


**Fig. 3.** S-type model. (a) shows original state. (b) is the compressed state. (c) illustrates the wrinkling state.

$$u_f = a_c + b_c x - \frac{h_s E_s}{h_f E_f} \left( c_c e^{\sqrt{\beta_x}} + d_c e^{-\sqrt{\beta_x}} \right) x_A \leq x < x_B. \quad (7b)$$

According to the stress continuity ( $\sigma_s|_{x_c(0 \leq x < x_c)} = \sigma_s|_{x_c(x_c \leq x < x_D)}$ ,  $\sigma_f|_{x_A(0 \leq x < x_A)} = \sigma_f|_{x_A(x_A \leq x < x_B)}$ ) in joint point between the contact region and the non-contact one, the displacement fields (Eq. (7)) and the corresponding stress fields then can be obtained by the geometric equations and constitutive relations. Similarly, the strain and displacement continuities are given in Eq. (8). Here, because the load is only applied to the substrate, the stress at the film boundary (point B in Fig. 2(a)) equals to the zero. Finally, detailed expressions of the displacement fields and the corresponding stress fields are shown in the supplementary materials (Note S1).

$$\sigma_s|_{x_c(0 \leq x < x_c)} = \sigma_s|_{x_c(x_c \leq x < x_D)}, u_f|_{x_A(0 \leq x < x_A)} = u_f|_{x_A(x_A \leq x < x_B)}. \quad (8a)$$

$$\epsilon_s|_{x=x_D} = \epsilon_0, \epsilon_f|_{x=x_B} = 0. \quad (8b)$$

Then, as shown in Fig. 3(c), the film will wrinkle when the compressive strain reaches to the critical value  $\epsilon_c$ . The film is considered to be clamped at two sides (points A in Fig. 2). The wrinkling behaviors are studied based on the nonlinear buckling theory of the elastic plate. The governing equation of the wrinkled film is:

$$D \nabla^4 w = \sigma_x \frac{\partial^2 w}{\partial x^2} + \sigma_y \frac{\partial^2 w}{\partial y^2} + 2\tau_{xy} \frac{\partial^2 w}{\partial x \partial y}. \quad (9)$$

where  $D$  is the flexural rigidity of the film. Due to same deformation along the y direction, Eq. (9) can be rewritten as a fourth-order ordinary differential equation.

$$\frac{d^4 w}{dx^4} - \frac{h_f}{D} \sigma_x \frac{d^2 w}{dx^2} = 0. \quad (10)$$

Based on the clamped boundary conditions:  $w|_{x=\pm x_A} = 0, w'|_{x=\pm x_A} = 0$ , the critical wrinkling stress  $\sigma_c$  applied to the film at  $x = \pm x_A$  and the deflection after the film is wrinkled then can be obtained as:

$$\sigma_c = \frac{E_f \pi^2}{12} \left( \frac{h_f}{x_A} \right)^2. \quad (11)$$

$$w = \frac{h_f}{\sqrt{3}} \left( 1 + \cos \left( \frac{\pi}{x_A} x \right) \right) \sqrt{\frac{\sigma|_{x=\pm x_A}}{\sigma_c} - 1}. \quad (12)$$

The Green strain is used here to describe the large deformation of the film. And, the linear constitutive relation of the film can be represented as [27]:

$$\sigma'_f = E_f \frac{du'_f}{dx} = E_f \left( \frac{du_f}{dx} + \frac{1}{2} \left( \frac{\partial w}{\partial x} \right)^2 \right). \quad (13)$$

Here,  $u'_f$  is the displacement of the film induced by compression and bending. The equilibrium equations of the substrate surface (Eq. (1)) and the film (Eq. (2)) in the contact region can then be rewritten as:

$$\text{substrate surface : } h_s E_s \frac{d^2 u_s}{dx^2} = \rho k \left( u_s - u'_f \right) x_C \leq x \leq x_D. \quad (14a)$$

$$\text{film : } h_f E_f \frac{d^2 u'_f}{dx^2} + \rho k \left( u_s - u'_f \right) = 0 x_A \leq x < x_B. \quad (14b)$$

The treatment of Eq. (14) is the same as that of Eq. (5). The displacement and stress fields of the substrate surface and the film can then be obtained according to the displacement compatibility ( $u_s|_{x_C(0 \leq x < x_c)} = u_s|_{x_C(x_C \leq x < x_D)}, u'_f|_{x_A(0 \leq x < x_A)} = u'_f|_{x_A(x_A \leq x < x_B)}$ ) and strain boundary conditions ( $\epsilon_s|_{x=x_D} = \epsilon_0, \epsilon_f|_{x=x_B} = 0$ ). The detailed expression of displacement and stress fields are shown in the supplementary materials (Note S1).

## 2.4. Description of the C-type film/substrate model

As shown in Fig. 1(c) and described in Section 2.3, the amplitude of wrinkle increases with increasing the compressive strain until the wrinkle contacts with the rigid plates. The following deformation of the film consists of three processes, including the point contact with the rigid plates (Fig. 4(b)), line contact (Fig. 4(c) and Fig. 4(e)) and the mode transition (Fig. 4(d) and Fig. 4(f)).

As shown in Fig. 4(a), the amplitude of wrinkle obtained from S-type model increase with the increasing of compressive strain. The point contact between the film and rigid plates occurs once the amplitude reaching  $h$ , as shown in Fig. 4(b). The frictionless contact assumption is adopted here to simplify the models. Moreover, effects of the complex contact conditions that film making contact with rigid plates can be referred to the reference [29]. Then, with the increase of the compressive strain, the contact region increases, causing the mode shifting from point contact to line contact, as shown in Fig. 4(c). The flat state of line contact region (no curvature and thus no bending moment) gives the boundary conditions:

$$w|_{x=l_1/2} = h, w|_{x=x_A} = w'|_{x=x_A} = w''|_{x=x_A} = w'|_{x=l_1/2} = w''|_{x=l_1/2} = 0, \quad (15)$$

Here, the line contact region is defined as the region that the film makes contact with the rigid plates. The deflection equation shown in Eq. (10) and the boundary condition in Eq. (15) require that the deflection of the film in the no-contact region ( $l_1/2 \leq x \leq x_A$ ) satisfy:

$$\frac{w}{h} = \frac{-2\pi(x - x_A)/(x_A - l_1/2) + \sin(2\pi(x - x_A)/(x_A - l_1/2))}{2\pi} \quad l_1/2 \leq x \leq x_A, \quad (16)$$

The relationship between the geometric parameters of the contact region and the applied stress to the film at  $x = \pm x_A$  should satisfy the following expression by combining Eq. (16) and Eq. (10):

$$\sigma|_{x=\pm x_A} = \frac{E_f h_f^2}{12} \left( \frac{2\pi}{x_A - l_1/2} \right)^2, \quad (17)$$

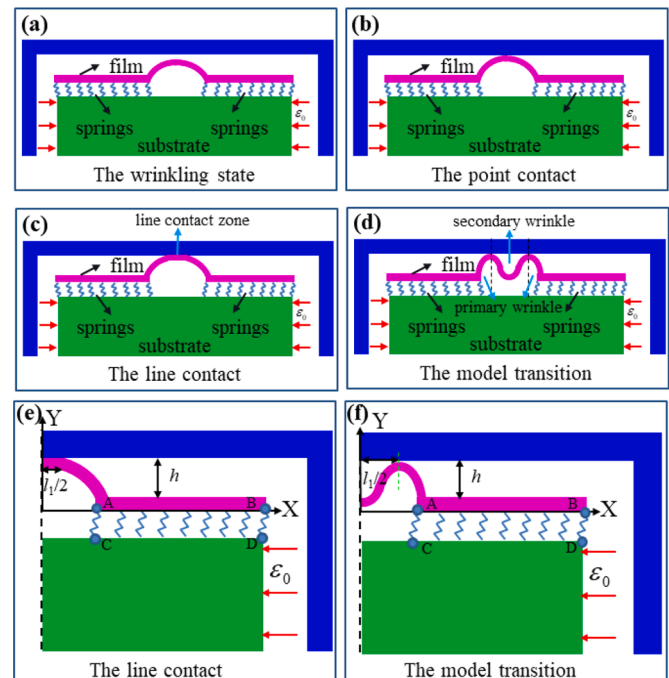


**Fig. 4.** C-type model. (a) shows wrinkling state obtained from S-type model. (b) illustrates point contact with the rigid plates. (c) is line contact. (d) shows the mode transition. (e) defines the geometric parameters in the line contact state. (f) defines the geometric parameters in the mode transition.

Moreover, according to the treatment of the equations in [Section 2.3](#), the displacement and stress fields of the substrate surface and the film can be obtained due to the displacement compatibility ( $u_s|_{x_c(0 \leq x < x_c)} = u_s|_{x_c(x_c \leq x < x_D)}$ ,  $u'_f|_{x_A(0 \leq x < x_A)} = u'_f|_{x_A(x_A \leq x < x_B)}$ ) and strain boundary conditions ( $\varepsilon_s|_{x=x_D} = \varepsilon_0$ ,  $\varepsilon'_f|_{x=x_B} = 0$ ). The detailed expressions are given in the supplementary materials (Note S1).

Moreover, as a special case of the line contact ( $l_1/2 = 0$ ), the point contact state is different from the end of the wrinkling state when the amplitude of the wrinkle is  $h$ . Thus, the displacement and stress fields of the substrate and the film in the point contact process can be obtained by taking  $l_1/2 = 0$  to the Eq. (5 s) and Eq. (6 s), which are detailed in the supplementary materials (Note S1).

Finally, when the line contact region is long enough, the mode transition occurs and the wrinkle of the film will snap as shown in [Fig. 4\(d\)](#). Here, as shown in [Fig. 4\(c\)](#) and [Fig. 4\(e\)](#), the film in the line contact region ( $-l_1/2 \leq x \leq l_1/2$ ) can be considered as the plates with clamped ends. Then, the critical wrinkling stress and the configuration of the wrinkle can be obtained according to the nonlinear buckling theory of the elastic plate. Therefore, as shown in [Fig. 4\(d\)](#) and [Fig. 4\(f\)](#), the transitioned model of the film consists of two parts, including the primary wrinkle ( $-x_A \leq x \leq -l_1/2$ ,  $l_1/2 \leq x \leq x_A$ ) and the secondary wrinkle ( $-l_1/2 \leq x \leq l_1/2$ ). Due to the symmetry of geometry and loading, as shown in [Fig. 4\(f\)](#), the boundary conditions can be expressed as:

$$w|_{x=l_1/2} = h, w|_{x=x_A} = w'|_{x=x_A} = w''|_{x=x_A} = w'|_{x=l_1/2} = w''|_{x=l_1/2} = 0, \quad (18)$$

Then, the deflection of the wrinkled film should satisfy:

$$w = h - \frac{h_f}{\sqrt{3}} \left[ 1 + \cos \left( \frac{\pi x}{l_1/2} \right) \right] \sqrt{\frac{\sigma|_{x=l_1/2}}{\sigma'_c} - 10} \leq x \leq l_1/2, \quad (19a)$$

$$\sigma'_c = \frac{E_f h_f^2}{12} \left( \frac{\pi}{l_1/2} \right)^2, \quad (19b)$$

$$\frac{w}{h} = \frac{-2\pi(x-x_A)/(x_A-l_1/2) + \sin(2\pi(x-x_A)/(x_A-l_1/2))}{2\pi} \quad l_1/2 \leq x \leq x_A, \quad (19c)$$

$$\sigma''_c = \frac{E_f h_f^2}{12} \left( \frac{2\pi}{x_A - l_1/2} \right)^2, \quad (19d)$$

Here,  $\sigma'_c$  is the critical mode transition stress of the film at  $x = l_1/2$  and  $\sigma''_c$  is the critical mode transition stress of the film at  $x = x_A$ . Moreover, the displacement and stress fields can be obtained due to the displacement compatibility ( $u_s|_{x_c(0 \leq x < x_c)} = u_s|_{x_c(x_c \leq x < x_D)}$ ,  $u'_f|_{x_A(0 \leq x < x_A)} = u'_f|_{x_A(x_A \leq x < x_B)}$ ) and strain boundary conditions ( $\varepsilon_s|_{x=x_D} = \varepsilon_0$ ,  $\varepsilon'_f|_{x=x_B} = 0$ ). The expressions are described in the supplementary materials (Note S1).

In addition, the boundary change is also considered in this paper. As discussed in [Section 2.1](#), the local springs will break when the displacement differences ( $u_s - u_f$ ) of the film and the elastic substrate surface in the contact region are greater than the critical failure displacement ( $\delta_c$ ). Thus, the boundary of the contact region will change with increasing the compressive load. The expression of the displacement and stress fields are described in the supplementary materials (Note S3).

### 3. The solution method of different models of film wrinkling

For the B-type model, as discussed in [Section 2.2](#), the analytical solution can be obtained. Once the interfacial sliding is introduced, however, as shown in [Sections 2.3](#) and [2.4](#), the displacement and stress fields of the S-type model are related to the boundary coordinates of the contact region. Due to the changing boundaries in the contact region, the analytical expression of displacement and stress fields can only be

iterated by the numerical method. Especially, when the lateral constraints are introduced, the analytical expression of displacement and stress fields (C-type model) cannot be directly obtained. As discussed in the supplementary materials (Note S1), the numerical iteration can only be processed when appropriate parameters  $c_1$  and  $c_m$  are selected based on the actual situation.

As defined in [Figs. 1, 2](#) and [4](#), the geometrical and material parameters of the film and the substrate are set as:  $\frac{L_f}{h_f}, \frac{b_c}{h_f}, \frac{h_f}{h_f} = 80, 20, 1$ ,  $\frac{L_s}{h_f}, \frac{b_s}{h_f}, \frac{h_s}{h_f} = 80, 20, 100$ ,  $\frac{x_A}{h_f}, \frac{x_B}{h_f}, \frac{x_C}{h_f}, \frac{x_D}{h_f} = 20, 40, 20, 40$ ,  $\frac{h}{h_f} = 2$ ,  $\frac{\delta_c}{h_f} = 1$ ,  $\frac{E_f}{E_s} = 250$  and  $\frac{\rho k h_f}{E_s} = 12.5$ , where  $h_f$  and  $E_s$  are taken as the length and the strength units, respectively. The solving processes are outlined in the form of the flow diagram, as shown in [Fig. 5](#). Considering the geometric parameters defined above, the film and elastic substrate surface are separated into 4000 material points. Moreover, due to the symmetry, only half of model (2000 material points) is considered in the calculation and their initial coordinates are from 0 to 40 ( $0 \leq \frac{x}{h_f} \leq 40$ ). Therefore, the left (A, C) and right (B, D) boundaries of the contact region correspond to the 1000th and 2000th material points of the film and the elastic substrate surface, respectively. The initial coordinates of these material points are:  $\frac{x_A}{h_f} = 20$ ,  $\frac{x_B}{h_f} = 40$ ,  $\frac{x_C}{h_f} = 20$ ,  $\frac{x_D}{h_f} = 40$ . And, 1000 local springs that connect the film and the elastic substrate are set in the contact region. The solution of the wrinkling, point contact, line contact and mode transition processes are similar to that of the compressed process except for the criterion for entering the next process. Therefore, the solution diagrams for these four processes are illustrated detailly in the supplementary materials (Note S2).

[Fig. 5](#) shows the solving diagrams of the film in the compressed process. Six steps are included in the solving processes.

- (1) Firstly, for the compressed process, the initial geometric parameters of the film and the elastic substrate surface in the contact region, initial strain and the iteration parameters are set as:  $x_A/h_f = 30$ ,  $x_B/h_f = 40$ ,  $x_C/h_f = 30$ ,  $x_D/h_f = 40$ ,  $\varepsilon_0 = 0$ ,  $i_1 = 0$ .
- (2) Considering a small increment of the strain  $\Delta\varepsilon = 1 \times 10^{-5}$ , the displacement and stress fields of the film and the elastic substrate surface in the compressing process can be obtained based on the expressions (Eqs. (8 and 9)).
- (3) Considering that interfacial sliding occurs on the right boundary firstly, the right boundaries (B, D) in the contact region will change. If the displacement differences of the right boundary ( $|x_B - x_D|$ ) are greater than the critical failure displacement ( $\delta_c$ ), the corresponding springs will break and the right boundaries (the 2000th material point) will be replaced by the new boundaries corresponding to the (2000-i1)th material point. As a result, the new coordinates of the right boundaries can be expressed as:  $x_B = (40h_s - 0.02h_s i_1) - u_f(2000 - i_1)$ ,  $x_D = (40h_s - 0.02h_s i_1) - u_s(2000 - i_1)$ . Here, the expressions  $u_f(2000 - i_1)$  and  $u_s(2000 - i_1)$  represent the displacement of the (2000-i1)th material point of the film and the substrate, respectively.
- (4) Because 1000 local springs are set between the film and the substrate surface, the interface interaction will fail when all these springs are broken, resulting in the end of the flow diagrams. Thus, the judging criterion is that whether the iteration parameter is less than 1000 ( $i_1 \leq 1000$ ).
- (5) When the coordinates of the new boundaries are obtained, the parameters (a, b, c, and d) related to the displacement and stress fields can be obtained by taking the new boundary coordinates ( $x_A, x_B, x_C, x_D$ ) and applied strain to their expressions.
- (6) Repeat Steps 3, 4 and 5 until the determination condition is satisfied. Here, the stress of the film at the left boundary of the contact region  $x = x_A$  reaches to the critical wrinkling value:  $\sigma|_{x=x_A} = \sigma_c$ . After that, the deformation of the film comes into the wrinkling process.

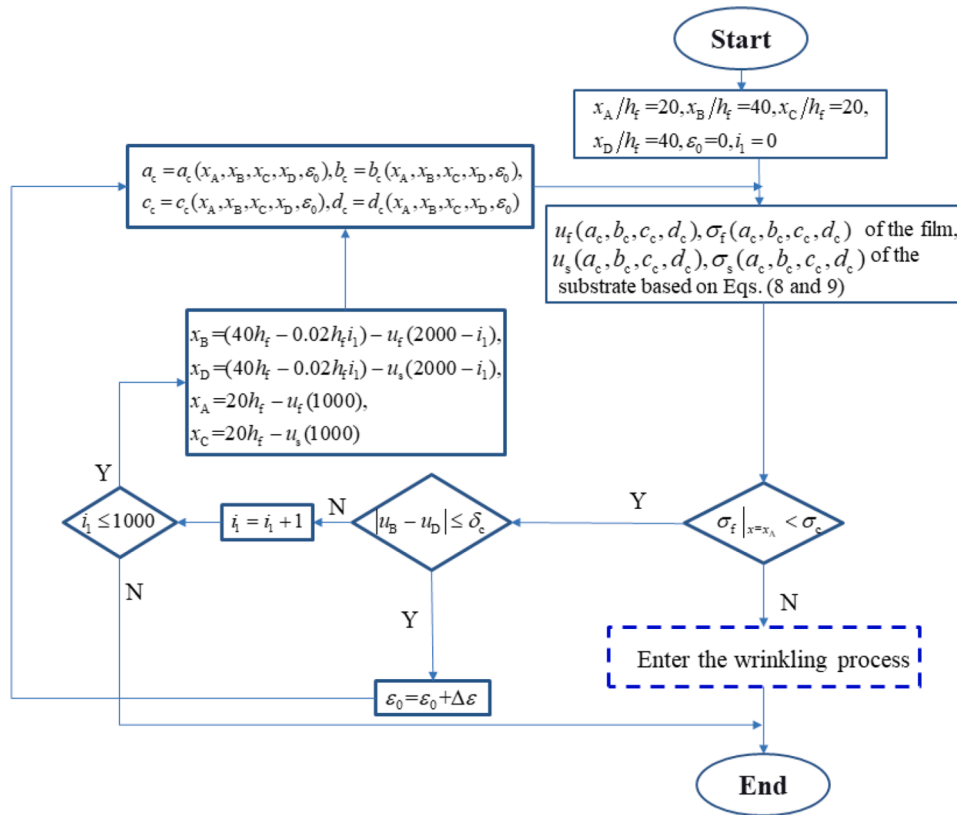


**Fig. 5.** shows the solving diagram of the compressed process.

Moreover, as discussed in [Section 2.4](#), the analytical expression of displacement and stress fields cannot be directly obtained for the C-type model. Especially, for the parameters  $c_l$  and  $c_m$  in the line contact and the mode transition process respectively, the numerical solutions are non-unique. Considering that the parameters  $c_l$  and  $c_m$  are continuous between the adjacent deformation states, they can be obtained by the continuity condition. Therefore,  $c_l$  is equal to  $c_p$  at  $\sigma|_{x=x_A} = \sigma_{cp}$ , which is the criterion for the deformation from point contact process to the line contact one.  $c_m$  equals  $c_l$  at  $\sigma|_{x=l_1/2} = \sigma_c$ , where the system deforms from the line contact process to the mode transition one.

#### 4. Results and discussions

##### 4.1. Deformation characteristics of the different models

As discussed in [Section 2](#), three different types of film wrinkling models can be included when the partial contact and the lateral constraint are considered. For the B-type system, the analytical solution can be obtained, while only the numerical solutions can be attained for the S-type and C-type systems. The numerical calculation method is illustrated detailedly in [Section 3](#). Fracture of the local springs is not included in this section and its effect is discussed in [Section 4.2](#). The calculation parameters are the same as those in [Section 3](#).

The deformation process is characterized by three types of film wrinkling models, as shown in [Fig. 6](#). The deformation of the B-type model includes two processes ([Figs. 6\(a and b\)](#)). Noted that the load is applied to both the film and the substrate, the applied strain is equal to the film strain at the left boundary of the contact region ( $\epsilon_0 = \epsilon_A$ ) due to the perfectly bonded assumption. The film wrinkles from flat state once the applied strain reaches the critical value ( $\epsilon_0 = \epsilon_c = \frac{\pi^2}{12} \left(\frac{h_f}{x_A}\right)^2 = 0.21\%$ ). After wrinkling, the stress of the left boundary ( $\frac{\sigma_A}{E_s}$ ) in the contact region and the deflection of the wrinkle ( $\frac{|w|}{h_f}|_{x=0}$ ) increase with

increasing of the applied strain. However, when the interfacial sliding and the lateral constraint are introduced, the deformation of the system proceeds through 5 phases, including the compressed state (I), the wrinkling state (II), the point contact state (III), the line contact state (IV) and the mode transition one (V). When the film stress of the left boundary ( $\sigma_A$ ) in the contact region reaches to the critical value ( $\frac{\sigma_A}{E_s} = \frac{\sigma_c}{E_s} = \frac{E_s h_f^2}{E_s 12} \left(\frac{h_f}{x_A}\right)^2 = 0.52$  in [Fig. 6\(a\)](#)), the film wrinkles (I-II) at applied strain 0.72%. In addition, the interfacial sliding will increase the critical strain applied to the elastic substrate compared to the B-type model. This attributes to the fact that stress distribution of the film and the elastic substrate surface in the contact region is no longer uniform and the strain of the left boundary ( $\epsilon_A, \epsilon_C$ ) is not equal to the strain applied to the substrate ( $\epsilon_0$ ) any more, which is different from the perfectly bonded interface case ([Figs. 6\(c and d\)](#)). After the film is wrinkled, its deflection will increase gradually to the distance between the film and the rigid plates  $h$  until point contact (II-III), where the corresponding applied strain is 3.53%. The line contact process starts once the stress of film in the left boundary ( $\sigma_A$ ) reaches to the critical value ( $\frac{\sigma_A}{E_s} = \frac{\sigma_{cp}}{E_s} = \frac{E_s h_f^2}{E_s 12} \left(\frac{2\pi}{x_A}\right)^2 = 2.12$  in [Fig. 6\(a\)](#)) (III-IV). Here, length of the line contact region is zero ( $l_1/2 = 0$ ) and the corresponding applied strain is 3.66%. And the length of the line contact region increases gradually until the film stress at the boundary of the line contact region reaches to the critical value ( $\frac{\sigma_{l_1/2}}{E_s} = \frac{\sigma'_c}{E_s} = \frac{E_s h_f^2}{E_s 12} \left(\frac{\pi}{l_1/2}\right)^2 = 4.93$ ) (IV-V), where the mode transition occurs and the secondary wrinkle appears in the film ( $\epsilon_0 = 7.94\%$ ). Finally, the computations are completed when the deflection of the second wrinkle is  $h$  ( $|w||_{x=0} = h$ ) and the applied strain is 15.85%. Moreover, a demonstrative experiment is conducted to illustrate the evolution of the constrained film, where the 5 processes ([Fig. 6\(g\)](#)) can be clearly observed. The detailed descriptions of the experiment are illustrated in the supplementary materials (Note S4 and

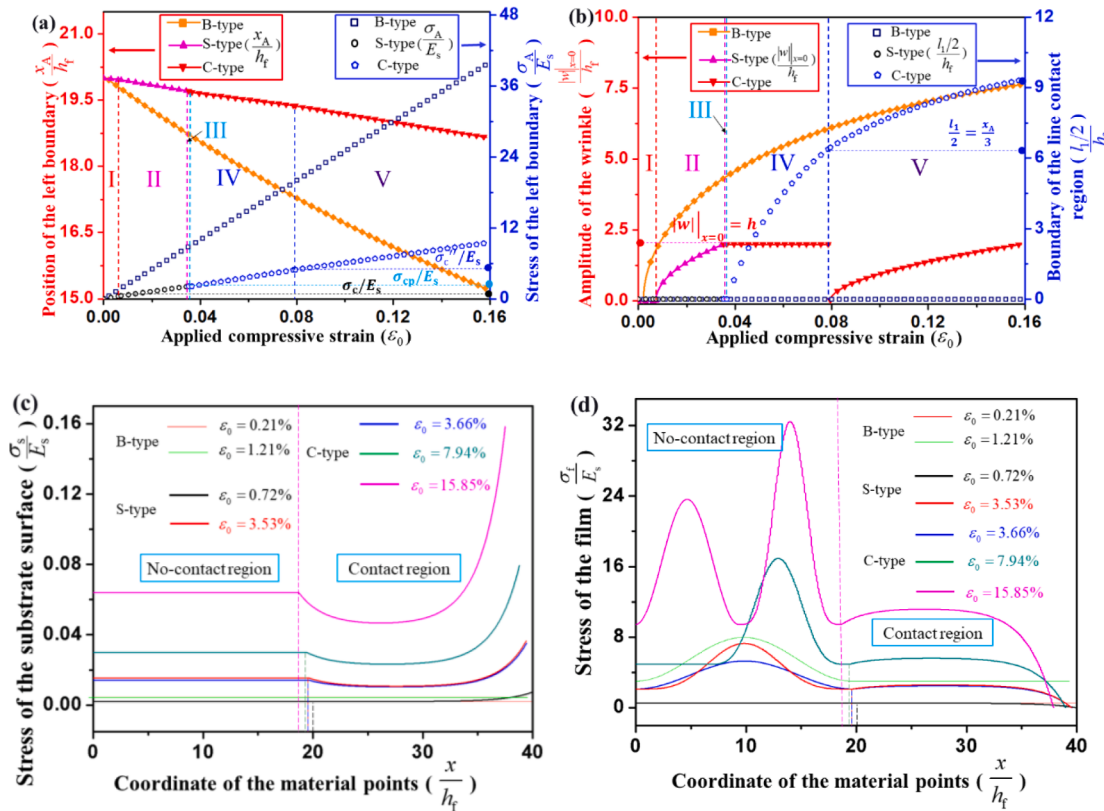


**Fig. 6.** Characterization of the deformation processes for three types of film wrinkling models. (a) the dimensionless coordinate ( $\frac{x_A}{h_f}$ ) as a function of the stress ( $\frac{\sigma_A}{E_s}$ ) at the left boundary (A in Fig. 2) of the contact region. (b) the dimensionless deflection of the wrinkle ( $\frac{|w|_{x=0}}{h_f}$ ), boundary of the line contact region ( $\frac{l_1/2}{h_f}$ ) versus the applied compressive strain ( $\epsilon_0$ ). (c) the stress of the elastic substrate surface. (d) film stress. (e) the displacement differences ( $\frac{u_s - u_f}{h_f}$ ) of the local springs at the critical strains for different deformation processes. (f) the configurations of the film and the elastic substrate surface at the critical strains. (g) Profiles of the film in the demonstrative experiment.

### Video 1.

As shown in Fig. 6(a), the transition from wrinkling to the point contact state is noteworthy (II-III). Here, the wrinkle amplitude of the film reaches  $h$  in the wrinkling process and the starting point of the line contact process with only one point of the film making contact with the rigid plates is named as the point contact state. As shown in Fig. 6(f), although amplitudes of the wrinkle at the end of the wrinkling process ( $\epsilon_0=3.53\%$ ) and the point contact state ( $\epsilon_0=3.66\%$ ) are equal, they are two completely different states during the film deformation. Thus, it is an interval from the end of the wrinkling process to the point contact state, which is called as point contact process. In the point contact process, the applied strain increases from 3.53% to 3.66%. Another important thing to be noticed is the process from the line contact state to the mode transition one (IV-V). It is known that the mode transition occurs when the line contact region is long enough ( $-l_1/2 \leq x \leq l_1/2$ ) and the film stress in the boundary of line contact region reaches the critical value. According to Eq. (19b), when  $\sigma_{l_1/2}$  equals to  $\sigma_c$ , the wrinkle snaps and the secondary wrinkle appears, where the film stress in the left boundary of the contact region is given by Eq. (19d) ( $\sigma_A = \frac{E_s h_f^2}{12} \left( \frac{2\pi}{x_A - l_1/2} \right)^2$ ). Because the curvature of the

film at  $x = l_1/2$  is zero, the film stress at  $x = l_1/2$  ( $\sigma_{l_1/2} = \frac{E_s h_f^2}{12} \left( \frac{\pi}{l_1/2} \right)^2$ ) is equal to that at  $x=x_A$  ( $\sigma_{l_1/2} = \sigma_A$ ) based on the constitutive relation shown in Eq. (13). As a result, the length  $l_1/2$  is equal to  $\frac{x_A}{3}$  ( $l_1/2 = \frac{x_A}{3}$ ) when the mode transition occurs, which is verified in the numerical calculation as well. As shown in Fig. 6(b), when the wrinkle snaps, the

length of the line contact region is 6.46 ( $\frac{l_1/2}{h_f} = 6.46$ ), where the coordinate of left boundary of the contact region is 19.38 ( $\frac{x_A}{h_f} = 19.38$  in Fig. 6(a)).

Moreover, as shown in Figs. 6(c and d) for B-type model, applying load to both the film and the substrate and the bonded interface results in the constant stresses of the film and the elastic substrate surface in the contact region. However, when the interfacial sliding is introduced (S-type and C-type) and the load is applied only to the substrate, the distribution of stress of both the film and elastic substrate surface are no longer uniform. Therefore, the critical wrinkling strain for the B-type system ( $\epsilon_c=0.21\%$ ) is smaller than that of the S-type one ( $\epsilon_c=0.72\%$ ) when the interfacial sliding is introduced. Moreover, effects of the interfacial sliding on the stress distribution will increase continually although deformation of the film goes into the wrinkling process. As shown in Fig. 6(a), the film stress in the left boundary of the contact region ( $\sigma_A$ ) for the B-type model is larger than that for the S-type one after wrinkle appears.

In addition, as shown in Eq. (5), the stress gradient ( $\frac{d\sigma_f}{dx}, \frac{d\sigma_s}{dx}$ ) is proportional to the displacement difference ( $u_s - u_f$ ). As a result, the variation of the stress can be derived by the displacement differences shown in Fig. 6(e). Here, the load state is defined as follows. When  $u_s - u_f$  is less than  $-10^{-4}$ , between  $-10^{-4}$  and  $10^{-4}$  or larger than  $10^{-4}$ , the corresponding spring exerts stretch load, keeps natural state or applies compressive load to the film. Thus, in the compressed process, some springs exert compressive load to the film and the others keeps natural state. When wrinkles appear, some springs that close to the wrinkle will transfer stretch load to the film. As the deformation of the system continues, more and more springs exert stretch load to the film. This

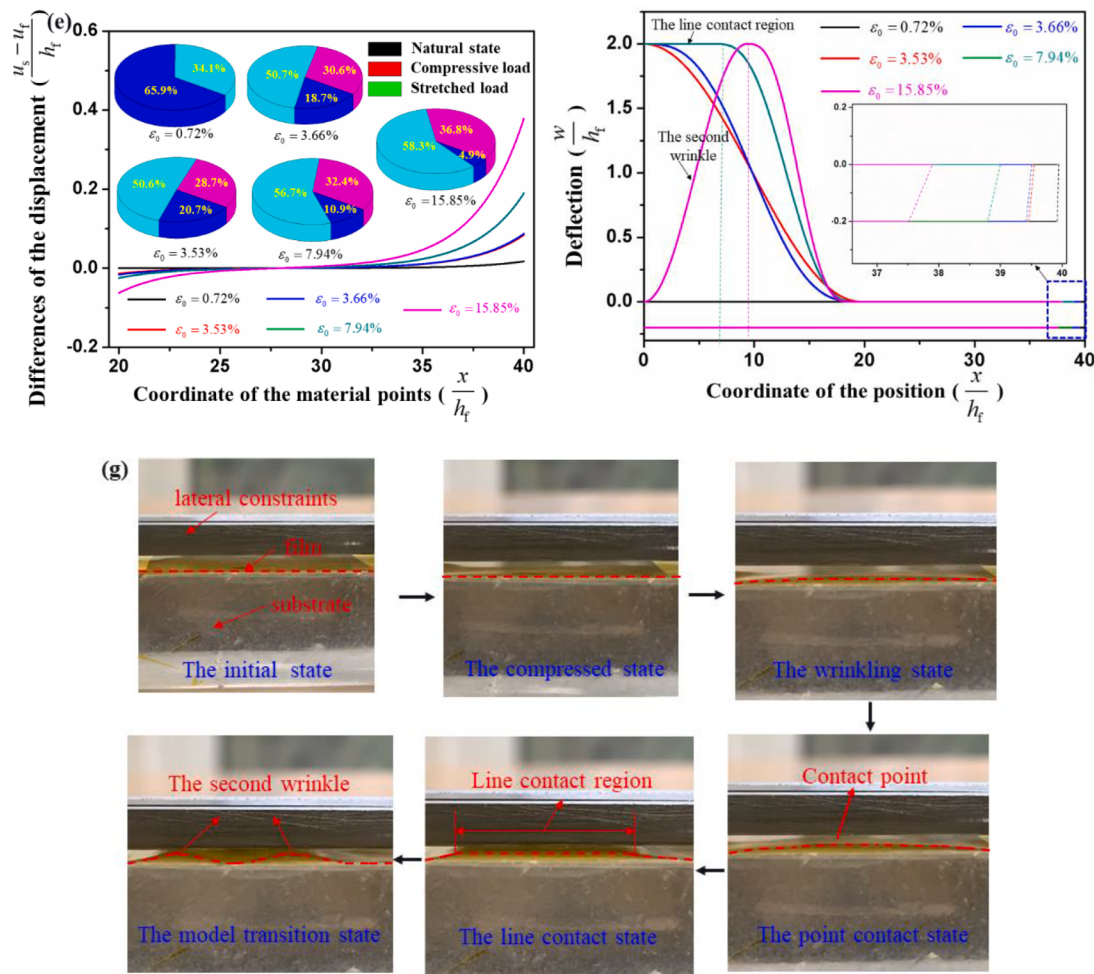


Fig. 6. (continued).

phenomenon is beyond our expectation because the wrinkle will be suppressed by the springs exerting stretch load. In fact, the appearance of springs exerting stretch load attributes the wrinkle. According to the expression of the Green strain in Eq. (15), the film strain includes two parts, which are the compression strain and the strain induced by the out-of-plane displacement ( $w$ ). While, the elastic substrate strain only includes the compression one. As a result, displacement of the film ( $u_f$ ) close to the wrinkle is larger than that of the substrate ( $u_s$ ). Moreover, as shown in Figs. 6(d), although some springs exerts stretch load to the film, the stress in the left boundary of the contact region ( $\sigma_A$ ) is still larger than zero, corresponding to the compressive load. Therefore, the phenomenon beyond our expectation is reasonable.

The configurations of the film and the elastic substrate surface under different applied strains are shown in Fig. 6(f). In the compressed process, the film and the elastic substrate surface remain flat. Under the wrinkling process, the film is wrinkled and the amplitude gradually increases to  $|w||_{x=0}=h$ . Here, it can be found that profiles of the film at the end of the wrinkling process and the point contact state are different, although they have the same maximum deflection ( $\frac{|w||_{x=0}}{h_f}=2$ ). When the line contact region length is long enough, the wrinkle will snap and the secondary wrinkle appears in the mode transition process. Here, due to the large thickness ratio of the substrate to the film ( $\frac{h_s}{h_f}=100$ ), the elastic substrate keeps flat during the whole deformation process. Moreover, as shown in the small box of Fig. 6(f), the displacement differences ( $u_s - u_f$ ) in the right boundary of the contact region increase with the deformation processing. In addition, the film profile changes are also verified by the demonstrative experiment in Fig. 6(g).

#### 4.2. Effect of the interfacial parameters on the deformation of the different film wrinkling models

##### 4.2.1. Effect of the interfacial strength

As discussed in Section 2.1, the interfacial strength can be represented by the critical failure displacement ( $\delta_c$ ) of the springs. When the interfacial stress exceeds the interfacial strength, the corresponding displacement differences ( $u_s - u_f$ ) will be larger than the critical value  $\delta_c$ , resulting in the interface fracture. Based on the results obtained in Fig. 6(e), the maximum displacement differences in critical states can be obtained. From state I to state II, II to III, III to IV, IV to V and V to the end of the calculation, the maximum displacement differences ( $\frac{u_s - u_f}{h_f}$ ) are 0.017, 0.084, 0.087, 0.190 and 0.379, respectively. The phase diagram of critical conditions for different film deformation states in terms of the maximum displacement difference and the applied compressive strain is shown in Fig. 7. The diagram characterizes the film deformation during the compressive strain increases, including the compressed process, wrinkling process, point contact process, line contact process, model transition process and interface fracture process.

According to the results obtained in Fig. 6(e), the maximum displacement difference appears in the right side of the contact region ( $\frac{u_s - u_f}{h_f}$ ), which is also the critical failure displacement ( $\frac{\delta_c}{h_f}$ ) of the springs at the interface. When the maximum displacement difference is below 0.017, the film deformation only experiences the compressed process. Here, all the springs will be broken successively when the applied strains reach to the critical values, resulting in the interface fracture. However, when the maximum displacement difference ranges from 0.017 to

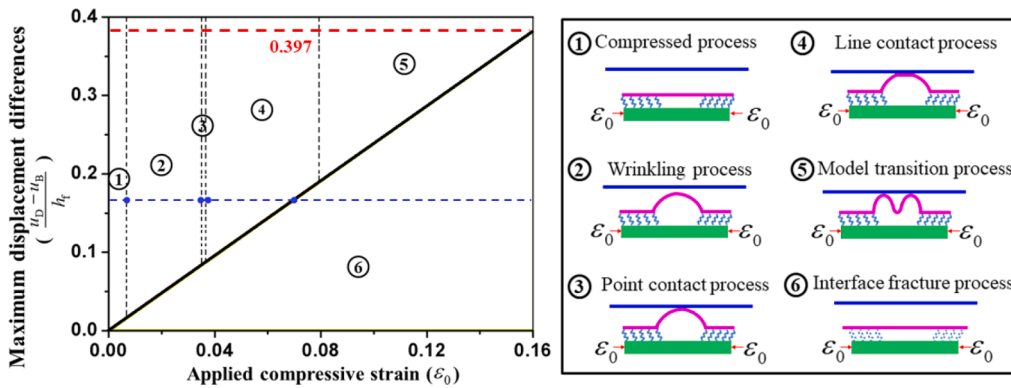


Fig. 7. Phase diagram of the effects of interfacial strength on the film deformation and different film deformation processes.

0.084, 0.084 to 0.087, 0.087 to 0.190 or 0.190 to 0.379, the film deformation is more complex but similar. Taking the film deformation with the maximum displacement difference being between 0.087 and 0.190 as an example, the film comes into the wrinkling, point contact and line contact states when the applied compressive strains are over 0.72%, 3.53% and 3.66%, respectively (dotted line in Fig. 7). Once the applied compressive strain reaching to the critical value (intersection of the dotted line and the green line), the interface fracture occurs. Here, the film deformation degenerates from the line contact state to the point contact state to the wrinkling state to the compressed one and finally returns to the initial state. Moreover, when the maximum displacement difference is greater than 0.379, the film will experience all the deformation states until the second wrinkle makes contact with the elastic substrate and the interface fracture will not occur.

#### 4.2.2. Effect of the interfacial stiffness

The interfacial stiffness is the production of the spring density and stiffness ( $pk$ ), which is discussed in Section 2.1. Based on the results shown in Fig. 6(a) and Fig. 7, it can be inferred that there is a critical interfacial stiffness in any deformation process defined in Section 4.1. When the interfacial stiffness is less than the critical value, the interface fracture will arise in this process. Otherwise, the film will enter the next deformation process. Moreover, the critical interfacial stiffness cannot be directly obtained and it can only be calculated by setting different values in the calculation. Here, the critical interfacial stiffness in the wrinkling process is discussed.

Fig. 8 shows the relationship between the interfacial stiffness and the critical wrinkling strain. For the B-type model, where the strain is applied to both of the film and the elastic substrate, the critical wrinkling

strain is a constant ( $\varepsilon_c = 0.21\%$ ) with the increase of the interfacial stiffness. For the film with bonded interface and the compressive strain is only applied to the elastic substrate, the critical wrinkling strain is larger ( $\varepsilon_c = 0.72\%$ ) and remains unchanged. As a result, applying load only to substrate raises the threshold of the film wrinkling. The square scatters are the results when the interfacial sliding is introduced and the compressive strain is only applied to the elastic substrate. With the decreasing of the interfacial stiffness, the critical wrinkling strain increases rapidly when the interfacial stiffness is less than 1 ( $\frac{\rho kh_f}{E_s} = 1$ ). Based on the calculation, all springs are broken before the wrinkle appears when the interfacial stiffness is set below 0.25 (unfilled square in Fig. 8), while the wrinkle will appear when the stiffness value is set as 0.29 (the first filled square in Fig. 8). Thus, the critical interfacial stiffness for entering in the wrinkling process can be inferred between 0.25 and 0.29 ( $0.25 < \frac{\rho kh_f}{E_s} \leq 0.29$ ).

#### 4.3. Effect of the length of the contact region

The effect of the initial contact region length on the deformation of the film is discussed in this section. According to the expressions of Eqs. (11), (12), (9s), (19b), and (19d), the critical film stresses in the left boundary of the contact region are  $\sigma_A = \frac{E_s \pi^2}{12} \left( \frac{h_f}{x_A} \right)^2$  for wrinkling,  $\sigma_A = \left( \left( \frac{\sqrt{3}h_f}{2h_s} \right)^2 + 1 \right) \frac{E_s \pi^2}{12} \left( \frac{h_f}{x_A} \right)^2$  for point contact,  $\sigma_A = \frac{E_s \pi^2}{3} \left( \frac{h_f}{x_A} \right)^2$  for line contact and  $\sigma_A = \frac{3E_s \pi^2}{4} \left( \frac{h_f}{x_A} \right)^2$  for the mode transition, respectively. It can be found that the critical film stress ( $\sigma_A$ ) in these deformation processes defined has the similar relationship with the initial contact region length ( $x_A$ ). Thus, the initial contact region length has the similar effect on any deformation process and its effect on the critical wrinkling strain is discussed as an example.

The effect of the initial contact region length ( $\frac{x_B - x_A}{h_s}$ ) on the critical wrinkling strain ( $\varepsilon_c$ ) is illustrated in Fig. 9. For the relatively small contact region (I and  $0 < \frac{x_B - x_A}{h_s} \leq 0.16$ ), as shown in Fig. 9(a), the critical wrinkling strain decreases with the increasing the initial contact region. The reason for the decreasing critical wrinkling strain ( $\varepsilon_c$ ) is that more springs participate the load transfer when the initial contact region increases. For state II ( $0.16 < \frac{x_B - x_A}{h_s} \leq 24$ ), the critical wrinkling strain shows slow increase because the critical wrinkling stress of the left boundary ( $\sigma_A$ ) increases slowly. In state III ( $24 < \frac{x_B - x_A}{h_s} \leq 36.8$ ), although more springs are set in the interface for increased initial contact region length, the critical wrinkling stress of the left boundary ( $\sigma_A$ ) increases more quickly due to the inverse relationship with the square of the initial contact region length ( $x_A$ ) shown above. As a result, the critical wrinkling strain ( $\varepsilon_c$ ) increases rapidly in this stage. After the contact region is long enough (IV and  $36.8 < \frac{x_B - x_A}{h_s} < 40$ ), wrinkle will not appear in the

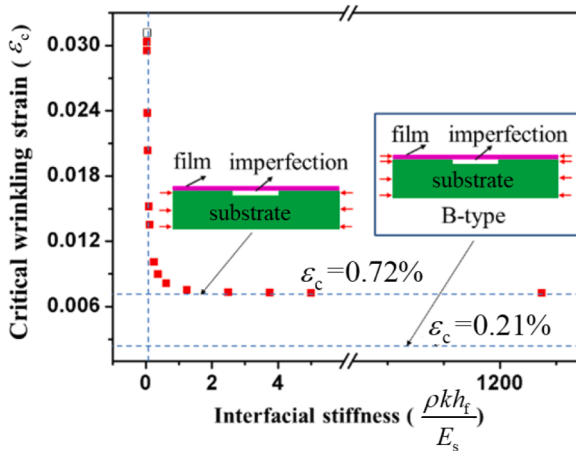
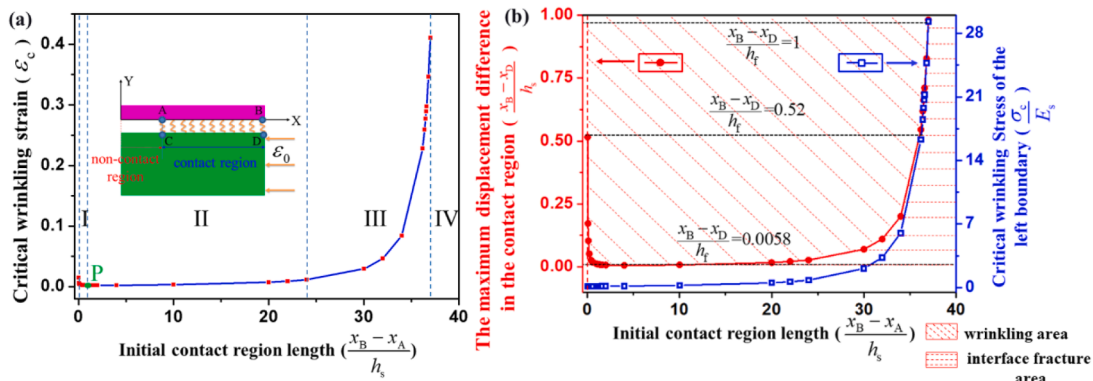


Fig. 8. Effect of the interfacial stiffness ( $\frac{\rho kh_f}{E_s}$ ) on the critical wrinkling strain ( $\varepsilon_c$ ).



**Fig. 9.** Effect of the initial contact region length ( $\frac{x_B - x_A}{h_s}$ ). (a) shows the change of the critical wrinkling strain ( $\epsilon_c$ ) with the initial contact region length. (b) is a phase diagram illustrating the conditions for appearing wrinkle or interface fracture. Also, it shows the relationship between the initial contact region length and the maximum displacement difference ( $\frac{x_B - x_D}{h_s}$ ), the critical wrinkling stress ( $\frac{\sigma_c}{E_s}$ ) of the left boundary of the contact region (A in Fig. 2).

film because the maximum displacement in the contact region ( $\frac{x_B - x_A}{h_s}$ ) reaches the critical value  $\delta_c$  and all springs will be broken successively.

The results can be discussed further for different interfacial strength. The maximum displacement differences in Fig. 9(b) are the values where the wrinkle just appears. As shown in Fig. 9(b), the minimum value of the maximum displacement difference is 0.0058, which is the minimum interfacial strength of wrinkle. Less than the minimum interfacial strength, the interface fracture occurs and the wrinkle will never appear in the film. For the interfacial strength ranging from 0.058 to 0.52, the wrinkle will appear in the film when the values are above the red line in Fig. 9(b), which corresponds to the slash area. While, when the values are below the red line, wrinkle will not appear (horizontal line area). This is due to the fact that there are not enough springs for the small contact region length or the critical wrinkling stress of the left boundary is too great for the larger contact region length. Moreover, for the large interfacial strength ( $0.52 < \frac{\delta_c}{h_s}$ ), the wrinkle will not appear only for the large contact region length (horizontal line area).

## 5. Model application

The developed model in previous sections is used to study the deformation of the graphene contacting to the polyethylene terephthalate (PET) substrate. For characterizing the deformation of the graphene, the parameters used in the calculations are picked out from the references and are listed in Table 1. Here, only the compressed and wrinkling processes are discussed because the interaction between the graphene and the rigid plates are more complex than the assumptions in our model.

The deformation characteristics of the graphene are illustrated in Fig. 10. As shown in Fig. 10(a), the change of the critical wrinkling strain with different contact region lengths is the same as that shown in Fig. 9

(a). For the small contact region ( $1\text{nm} \leq x_B - x_A < 3\text{um}$ ), the critical wrinkling strain decreases with the increasing contact region because more springs are set to participate the load transfer. However, the critical wrinkling strain increases sharply when the contact region length reaches a certain value although enough springs are set in the interface.

This attributes to the inverse relationship ( $\sigma_A = \frac{E_s \pi^2}{12} \left( \frac{h_f}{x_A} \right)^2$ ) between the second power of the initial non-contact region length ( $x_A$ ) and the critical wrinkling stress of the film ( $\sigma_A$ ). However, the phenomenon that the critical wrinkling strain decreases with increasing the contact region for small contact region is not be observed in Jiang's experiment [24] because this theoretical phenomenon appears when the applied strain is on the order of  $10^{-9}$ . In our calculation, the critical wrinkling strain is 0.25% and the maximum displacement difference is 4.3 nm when the non-contact region length is 7 nm. Our calculated results of the minimum non-contact region length for wrinkling are close to those from the references. For the graphene contacting with PET, the initial buckling length is 4.2 nm and the critical buckling strain is 0.26% based on Cui's calculation [8] and the initial buckling length is 2 nm by setting the critical wrinkling strain as 0.7% estimated by Jiang [24]. It can be found that these two results are close but less than our calculation values, which may due to the assumption in our models that the interfacial interaction is zero when the corresponding springs are broken while the interfacial interaction is considered as a constant when spring broken occurs in these two references.

The strain distribution of the graphene is shown in Fig. 10(b), where the non-contact region length is 7 nm. The strain distribution is characterized by the shear-lag effect and is the same as that of the experimental data [24] when the applied strain is 0.2%. Although the experimental data is obtained from stretching the graphene, they are comparable and the same as those obtained by compressing the graphene in the compressed process of our model. The spring broken occurs when the applied strain is 0.25% shown in Fig. 10a, which is close to the simulated or experimental values 0.3% [8,24].

For the graphene with 7 nm long non-contact region, the change of the critical wrinkling strain with the length of the graphene is shown in Fig. 10(c). The critical wrinkling strain shows the significant size effect when the length is less than 13 μm, while the size effect length of the graphene is 8 μm in Cui's calculation [8]. The reason has been explained in Fig. 10(a) that the constant interfacial interaction assumption in their calculation, which results in the smaller initial buckling length (4.2 nm). However, the reason for size effect is not illustrated in their work. In fact, the size effect is due to the shear-lag effect of the deformed graphene and the PET. For the graphene contacting to PET with a given non-contact region, the critical wrinkling strain of the graphene then can be determined by the expression ( $\epsilon_c = \frac{\pi^2}{12} \left( \frac{h_f}{x_A} \right)^2$ ). In addition, based on the results

**Table 1**  
Main parameters of the graphene, PET and interface in the present study.

Parameter	Definition	Value	Source
$E_f$	Young's modulus of graphene	1TPa	[28]
$\nu_f$	Poisson's ratio of graphene	0.16	[8]
$L_f \times b_f \times h_f$	Geometric dimensions of graphene	40, 10, 3.5 × $10^{-4}$ (μm)	[8]
$\rho k$	Stiffness of the interface	$\rho k = 100\text{TPa}/m$	[24]
$E_s$	Young's modulus of the PET	4GPa	PET
$\nu_s$	Poisson's ratio of the PET	0.4	PET
$\delta_c$	Critical failure displacement	5.5nm	[24]
$L_s \times b_s \times h_s$	Geometric dimensions of the PET	40, 10, 0.5(μm)	PET
$x_A, x_B$	Initial values defined in Fig. 2	10μm, 20μm	
$x_C, x_D$	Initial values defined in Fig. 2	10μm, 20μm	
$h$	Parameter defined in Fig. 4	1μm	

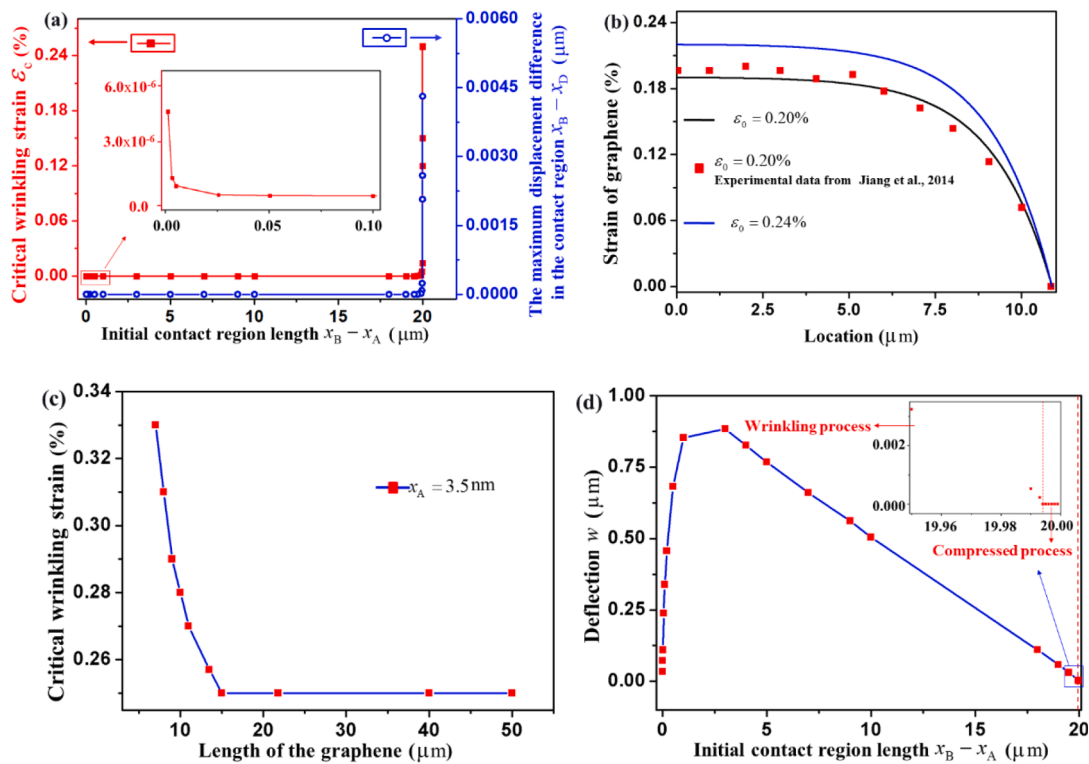


**Fig. 10.** Characteristics of the graphene deformation. (a) shows the change of the critical wrinkling strain ( $\varepsilon_c$ ) and the maximum displacement difference in the contact region ( $x_B - x_D$ ) with the initial contact region length. (b) shows the strain distribution of the graphene and the comparison with the experimental data from [24]. (c) illustrates the relationship between the critical wrinkling strain and the length of the graphene with 7 nm of the initial non-contact region ( $x_A = 3.5\text{nm}$ ). (d) expresses the maximum deflection of the graphene from different initial contact region when springs broken occurs in the interface.

shown in Fig. 6(e), the shear stress decreases from the edges and are close to zero at the center. For a longer graphene (greater than 13  $\mu\text{m}$ ), only the springs near the edge participate the load transfer and springs close to the center keep the natural state. However, for a short graphene, all the springs will participate the load transfer and the applied critical wrinkle strain increases with decreasing the graphene length.

For different initial contact region, the maximum deflection of the graphene when the spring broken occurs is calculated in Fig. 10(d). For the larger contact region ( $19.993\mu\text{m} \leq x_B - x_A$ ), the spring broken occurs without wrinkling in the compressed process and the reason is illustrated in Fig. 10(a) above. For the contact region ( $3\mu\text{m} \leq x_B - x_A < 19.993\mu\text{m}$ ), the maximum deflection of the graphene increases with the decreasing of contact region length, which is due to the decreasing critical wrinkling strain shown in Fig. 10(a). However, the maximum deflection of the graphene shows decreasing trend when the contact region length decreases from 3  $\mu\text{m}$  to 1  $\mu\text{m}$  because the corresponding critical wrinkling strain increases, which is also illustrated in Fig. 10(a). Moreover, the maximum deflection of the graphene is 0.88  $\mu\text{m}$  when contact region length is 3  $\mu\text{m}$ .

## 6. Conclusions

In summary, this paper performed theoretical analysis, numerical simulations and experimental measurement to address the wrinkling behaviors of the film with partial contact and lateral constraints being included especially. Due to the introduction of the lateral constraints, the film undergoes 5 processes, including the compressed state, the wrinkling state, the point contact state, the line contact state and the mode transition one. When the interface failure is considered, interface strength, interface stiffness and the length of the contact region contribute to the film deformation. Increasing the interfacial strength and stiffness will accelerate the film wrinkling and increase the interface failure threshold. For the initial contact region length, the film wrinkling

attributes to the competition of the spring number and the increasing rate of the film critical wrinkling stress. The spring number plays the major role for the small contact region length, otherwise it is the increasing rate of the wrinkling stress. For the graphene contacting with the PET, the critical wrinkling strain of the graphene shows significant size effect when the length is less than 13  $\mu\text{m}$ . This attributes the shear-lag effect because only the springs near the edge participate the load transfer for the graphene with length greater than 13  $\mu\text{m}$ , while all the springs will participate the load transfer when the length is less than 13  $\mu\text{m}$ .

## CRediT authorship contribution statement

**Mengxiong Liu:** Data curation, Writing – original draft, Formal analysis, Writing – review & editing, Investigation. **Zhiming Xue:** Validation, Investigation, Writing – review & editing. **Yafei Wang:** Validation, Visualization. **Xide Li:** Supervision, Funding acquisition. **Changguo Wang:** Conceptualization, Resources, Writing – review & editing, Project administration, Funding acquisition.

## Declaration of Competing Interest

The authors declare that they have no known competing financial interests or personal relationships that could have appeared to influence the work reported in this paper.

## Acknowledgments

M.L. and C.W. acknowledge financial supports from National Natural Science Foundation of China, 11872160 and 12172102. M.L. and X.L. acknowledge financial supports from National Natural Science Foundation of China, 11872035 and 12172190.

## Supplementary materials

Supplementary material associated with this article can be found, in the online version, at doi:10.1016/j.ijmecsci.2021.107022.

## Reference

- [1] Bernal R, Tassius C, Melo F, Gémard JC. Mechanical characterization of elastic thin-films: cell mechanics applications. *Appl Phys Lett* 2015;90:063903.
- [2] Bowden N, Brittain S, Evans AG, Hutchinson JW, Whitesides GM. Spontaneous formation of ordered structures in thin films of metals supported on an elastomeric polymer. *Nature* 1998;393:146–9.
- [3] Cai S, Breid D, Crosby AJ, Suo Z, Hutchinson JW. Periodic patterns and energy states of buckled films on compliant substrates. *J Mech Phys Solids* 2011;59: 1094–114.
- [4] Chai H. The post-buckling response of a bi-laterally constrained column. *J Mech Phys Solids* 1998;46:1155–9.
- [5] Chan EP, Crosby AJ. Fabricating microlens arrays by surface wrinkling. *Adv Mater* 2010;18:3238–42.
- [6] Chen P, Chen S, Peng J. Interface behavior of a thin-film bonded to a graded layer coated elastic half-plane. *Int J Mech Sci* 2016;115:489–500.
- [7] Chen MW, Dutta I. Atomic force microscopy study of plastic deformation and interfacial sliding in Al thin film: Si substrate systems due to thermal cycling. *Appl Phys Lett* 2000;77:4298–300.
- [8] Cui Z, Guo JG. Theoretical investigations of the interfacial sliding and buckling of graphene on a flexible substrate. *AIP Adv* 2016;6:125110.
- [9] Gao X, Li C, Song Y, Chou TW. A continuum mechanics model of multi-buckling in graphene-substrate systems with randomly distributed debonding. *Int J Solids Struct* 2016;97:510–9.
- [10] Dai L, Gong J, Gu X. Failure analysis on interfacial slipping in a film/substrate structure. *Mech Eng Technol* 2013. 02113–117.
- [11] Dai L, Feng X, Liu B, Fang D. Interfacial slippage of inorganic electronic materials on plastic substrates. *Appl Phys Lett* 2010;97. 221903–221903–3.
- [12] Feng X, Yang BD, Liu Y, Wang Y, Dagdeviren C, Liu Z, Carlson A, Li J, Huang Y, Rogers JA. Stretchable ferroelectric nanoribbons with wavy configurations on elastomeric substrates. *ACS Nano* 2011;5:3326–32.
- [13] Giannaopoulos AE, Nilsson KF, Tsamaphyros G. The contact problem at delamination. *J Appl Mech* 1995;62:989–96.
- [14] Haftbaradaran H, Soni SK, Sheldon BW, Xiao X, Gao H. Modified stoney equation for patterned thin film electrodes on substrates in the presence of interfacial sliding. *J Appl Mech* 2012;79:031018.
- [15] Harris AK, Wild P, Stopak D. Silicone rubber substrata: a new wrinkle in the study of cell locomotion. *Science* 1980;208:177–9.
- [16] He S, Su Y, Ji B, Gao H. Some basic questions on mechanosensing in cell-substrate interaction. *J Mech Phys Solids* 2014;70:116–35.
- [17] Heide-Jørgensen S, Budzik MK. Effects of bondline discontinuity during growth of interface cracks including stability and kinetic considerations. *J Mech Phys Solids* 2018;117:1–21.
- [18] Holland MA, Li B, Feng XQ, Kuhl E. Instabilities of soft films on compliant substrates. *J Mech Phys Solids* 2017;98:350–65.
- [19] Huang R, Suo Z. Instability of a compressed elastic film on a viscous layer. *Int J Solids Struct* 2002;39:1791–802.
- [20] Huang X, Li B, Hong W, Cao YP, Feng XQ. Effects of tension-compression asymmetry on the surface wrinkling of film-substrate systems. *J Mech Phys Solids* 2016;94:88–104.
- [21] Huang Y, Chen H, Wu J, Feng X. Controllable wrinkle configurations by soft micro-patterns to enhance the stretchability of Si ribbons. *Soft Matter* 2014;10:2559–66.
- [22] Hutchinson JW, Suo Z. Mixed-mode cracking in layered materials. *Adv Appl Mech* 1992;29:63–191.
- [23] Ji B, Bao G. Cell and molecular biomechanics: perspectives and challenges. *Acta Mech Solida Sin* 2011;24:27–51.
- [24] Jiang T, Huang R, Zhu Y. Interfacial sliding and buckling of monolayer graphene on a stretchable substrate. *Adv Funct Mater* 2014;24:396–402.
- [25] Jin C, Khare K, Vajpayee S, Yang S, Jagota A, Hui CY. Adhesive contact between a rippled elastic surface and a rigid spherical indenter: from partial to full contact. *Soft Matter* 2011;7:10728–36.
- [26] Khang DY, Jiang HQ, Huang Y, Rogers JA. A stretchable form of single-crystal silicon for high-performance electronics on rubber substrates. *Science* 2006;311: 208–12.
- [27] Landau LD, Lifshitz EM. Theory of elasticity. Course of theoretical physics. 1986. p. 3.
- [28] Lee C, Wei X, Kysar JW, Hone J. Measurement of the elastic properties and intrinsic strength of monolayer graphene. *Science* 2008;321.
- [29] Liu M, Wang C, Li X. Rigid-flexible contact analysis of an inflated membrane balloon with various contact conditions. *Int J Solids Struct* 2018. S0020768318301896.
- [30] Liu Y, Guo K, Wang C, Han J, Gao H. Wrinkling and ratcheting of a thin film on cyclically deforming plastic substrate: mechanical instability of the solid-electrolyte interphase in li-ion batteries. *J Mech Phys Solids* 2018. S0022509618303028.
- [31] Manners W. Methods for analysing partial contact between surfaces. *Int J Mech Sci* 2003;45:1181–99.
- [32] McGarry JP, Murphy BP, McHugh PE. Computational mechanics modelling of cell-substrate contact during cyclic substrate deformation. *J Mech Phys Solids* 2005;53: 2597–637.
- [33] Pan K, Ni Y, He L, Huang R. Nonlinear analysis of compressed elastic thin films on elastic substrates: from wrinkling to buckle-delamination. *Int J Solids Struct* 2014; 51:3715–26.
- [34] Park S, Ahn J, Feng X. Theoretical and experimental studies of bending of inorganic electronic materials on plastic substrates. *Adv Funct Mater* 2008;18: 2673–84.
- [35] Qian J, Wang J, Gao H. Lifetime and strength of adhesive molecular bond clusters between elastic media. *Langmuir* 2008;24:1262–70.
- [36] Rogers JA, Someya T, Huang YG. Materials and Mechanics for Stretchable Electronics. *Science* 2010;327:1603–7.
- [37] Ruffini A, Durinck J, Colin J, Coupeau C, Grilhé J. Gliding at interface during thin film buckling: a coupled atomistic/elastic approach. *Acta Mater* 2012;60:1259–67.
- [38] Stafford CM, Harrison C, Beers KL, Karim A, Amis EJ, VanLandingham MR, Kim HC, Volksen W, Miller RD, Simonyi EE. A buckling-based metrology for measuring the elastic moduli of polymeric thin films. *Nat Mater* 2004;3:545–50.
- [39] Stopak D, Harris AK. Connective tissue morphogenesis by fibroblast traction. I. Tissue culture observations. *Dev Biol* 1982;90:383–98.
- [40] Strani M, Sabetta F. Free vibrations of a drop in partial contact with a solid support. *J Fluid Mech* 1984;141:233–47.
- [41] Wang C, Kang J, Xue Z, Tan H. Buckling induced delamination and microflow analysis of film/substrate system. *Compos Struct* 2017;161:8–14.
- [42] Xue Z, Wang C, Tan H. Articulated surface wrinkling of a patterned film with periodic stiffness distribution on a compliant substrate. *Int J Solids Struct* 2020; 200–1.
- [43] Yin SF, Li B, Cao YP, Feng XQ. Surface wrinkling of anisotropic films bonded on a compliant substrate. *Int J Solids Struct* 2018. S0020768318300799.
- [44] Young RJ, Kinloch IA, Gong L, Novoselov KS. Super-elastic graphene ripples for flexible strain sensors. *ACS Nano* 2011;5:3645–50.
- [45] Yu H H, Hutchinson JW. Influence of substrate compliance on buckling delamination of thin films. *Int J Fracture* 2002;113:39–55.
- [46] Zhang K, Arroyo M. Adhesion and friction control localized folding in supported graphene. *J Appl Phys* 2013;113:193501.
- [47] Zhang Y, Wang F, Ma Y, Feng X. Buckling configurations of stiff thin films tuned by micro-patterns on soft substrate. *Int J Solids Struct* 2019;161:55–63.